ABSORPTION RATE AND VOLUME DEPENDENCY ON THE COMPLEXITY OF POROUS NETWORK STRUCTURES

Patrick A. C. Gane, Cathy J. Ridgway* and Joachim Schoelkopf
Omya AG, CH-4665 Oftringen, Switzerland.

(Short title: Absorption Dependency on Porous Network Complexity)

ABSTRACT

Results of simulated supersource imbibition into model network structures are compared with experimental observations of real network structures determined by dynamical gravimetric fluid uptake. A computer model, Pore-Cor, has been used previously to simulate the imbibition of fluid into porous structures by applying an imbibition algorithm for fluids undergoing both inertial and viscous dynamical absorption (Schoelkopf *et al.*, Journal of Colloid and Interface Science, 227 (2000) 119). The structures comprise cubic pores connected by cylindrical throats on a three-dimensional 10x10x10 position matrix. The absorption curves for model structures with monosized pore and throat size ranges and for polydisperse pore and throat size distributions centred around 0.1 µm, increasing from 0.1 µm as a lower limit, and decreasing from 0.1 µm as an upper limit, respectively, are analysed. A relevant observable porosity and 50 % volume intrusion radius (r_{50}) are obtained using simulated mercury intrusion. Experimental network pore structures were made using compressed tablets, formed under a series of pressures, of two finely ground calcium carbonates with defined differences in skeletal particle size distribution. The surface chemical, particulate and morphological pore characteristics were maintained constant over a range of porosities using controlled wet grinding and careful use of dispersant levels such that the ratio of dispersant to BET surface area was held constant. The experimental porosities were determined by mercury intrusion porosimetry applying corrections for mercury compression and penetrometer expansion together with a correction for sample skeletal compression (Gane *et al.* Industrial and Engineering Chemistry Research, 35 (1996) 1753). The applicability of the Lucas-Washburn equation is examined by defining two equivalent hydraulic radii, one based on a Darcy absorption length ($r_{ehcDarcy}$) and the other on a volume uptake (r_{ehc}), respectively. The results from the model structures having distributions of pores and throats, which contain either small or large pores respectively, follow the experimental results qualitatively. Both approaches show a long timescale macroscopic absorption rate depending approximately, but not exactly, on the square root of time. The two experimental series, however, fail to scale with each other via the Lucas-Washburn equation in accordance with pore size, r_{50}. Porosity is shown to be the main factor determining the volume absorption rate, and, when used as a weighting factor, gives linear correlation-scaling between r_{50} and a derived volume-based r'_{ehc} equivalent hydraulic radius, obtained from an analytical expression of the observed Darcy-based $r_{ehcDarcy}$. The experimental samples showed that the directly observed r_{ehc} and the calculated r'_{ehc}, derived from Darcy length, were equal, but this was not the case for the model values. A factor $b = r'_{ehc}/r_{50}$ is shown to be a possible descriptor of the sample network complexity and an indicator for the probability level of pore filling during the absorption dynamic.

Keywords: absorption, network model, equivalent hydraulic radius, Lucas-Washburn, imbibition, complexity factor

* Author to whom correspondence should be addressed

INTRODUCTION

Imbibition of fluids by porous network structures plays an important part in many industrial and environmental applications including oil recovery, water distribution in soil substrates, the manufacture of surface coatings, the application of fluid-based paints and lacquers, and the printing of paper. The long-accepted Lucas-Washburn equation relates the volume rate of fluid uptake by a capillary to the Laplace pressure difference across a meniscus derived from the wetting contact force of the fluid for the capillary wall with a resistive viscous Poiseuille flow simultaneously acting to retard the uptake. This approach has frequently been shown to have shortcomings when considering short timescales especially in pore structures with fine (short) elemental structures, such as might be found in fine sedimentary deposits or in finely structured pigmented coatings (Taylor *et al.*, 2000; Einset, 1996; Yang *et al.*, 1988; van Oss *et al.*, 1992; Dube *et al.*, 2000; Quere, 1997; Li *et al.*, 1994; Fisher *et al.*, 1979; Chibowski *et al.*, 1997; Gane *et al.*, 2000; Schoelkopf *et al.*, 2000a; Schoelkopf *et al.*, 2000b). This is generally considered to be due to the acceleration experienced by a column of fluid entering the capillary or element. Various models have been applied to the problem ranging from classical mechanics, including momentum (inertia) (Bosanquet, 1923) and energy conservation (Szekely *et al.*, 1971; Levine *et al.*, 1976; Letelier *et al.*, 1979; Batten, 1984; Ichikawa *et al.*, 1994; Marmur *et al.*, 1997), to molecular dynamics based on individual interactive forces between molecules and between the molecular ensemble and the capillary wall (Martic *et al.*, 2000). All approaches have various drawbacks. The classical approaches, by definition, cannot accurately describe instantaneous impulse effects without resorting to integrals spanning the initial start of imbibition (Bosanquet, 1923), or there is an unknown energy balance between the imbibing fluid and that within the fluid bulk reservoir (Szekely *et al.*, 1971). The molecular dynamics approaches are as yet limited by computing power and particle number and are not applicable to upscaling in a realistic network model.

One of the earliest approaches to analyse imbibition was reported by Bell and Cameron (1906) who found a square-root dependency of time for absorption which was also found, apparently independently, by Ostwald (1908). The best-known solution was introduced by Lucas (1918) and Washburn (1921), which combined the Laplace relation with Poiseuille's equation of laminar flow. The lack of inertial terms, relating to the mass of fluid under motion, was recognised by Rideal (1922). Bosanquet (1923) complemented Rideal's solution in 1923, adding the inertial impulse drag effect associated with an accelerating fluid.

Szekely *et al.* (1971) (not referring to Rideal or Bosanquet) started from an energy balance and removed the initial infinity of the Lucas-Washburn velocity. Letelier (1979) mentioned that, stripped of arbitrarily added corrective terms, their equation is identical with that of Bosanquet.

Levine *et al.* (1976) introduced a sink flow towards the capillary entrance from the reservoir, referring to Szekely and adding some changes or improvements. They focussed on the low Reynolds number regime which they considered to be more practically relevant. Levine *et al.* (1980) account for the deviation from Poiseuille flow in the vicinity of the moving meniscus by including a slip condition. Letelier *et al.* (1979), (also not referring to Levine's papers) started from the Navier-Stokes equations, discussing both Szekely's and Bosanquet's work. They identified an incorrect coefficient in the second order term, and claimed to have given a more rigorous solution, with dimensionless variables, in the form of a series expansion. Batten (1984) (not referring to Levine's papers) accepted Letelier's and Szekely's efforts as rigorous but remarked on their disagreement with experimental data. He added to Szekely's

equation the dissipation of a kinetic energy head and the initial establishment of a dynamic contact angle. He claimed that the Letelier approach ignored the correction for converging flow at the capillary entry. He compared his own equation, and the two others mentioned, with data from LeGrand and Rense (1945). Ichikawa and Satoda (1994) (not referring to Levine's 1979 work) claimed that Letelier did not account for inertia during the inlet acceleration. They started with an energy balance and arrived at an extended dimensionless Bosanquet relation. Marmur and Cohen (1997) in turn separated surface tension and radius for individual analysis using an equation for vertical capillarity without specifying the origin. Moshinskii (1997), only referring to Russian authors, solved the Navier-Stokes equations using advanced methods to obtain an integro-differential equation. He did not consider the effects at the ends of the liquid column he described. When any of these latter equations are applied to a porous substrate, the number of unknown parameters tends to grow unmanageably.

It is with such a background that the work here is focussed on the following authors. First of all, the initial approach of Lucas (1918) and Washburn (1921) and then the classical mechanical approach of Bosanquet (1923) as taken further by Schoelkopf *et al*. (2000a) and Ridgway *et al.* (2001).

Competitive effects in a range of interconnected pores are included in the model presented here, and provide the distinctive difference between the classical approach of a bundle of capillaries derived from the Laplace intrusion pressure of mercury and the more realistic network approach. A computer network model, Pore-Cor[1], has been used to simulate the imbibition of fluid into porous structures by applying an imbibition algorithm for fluids undergoing both inertial and viscous dynamical absorption. The evidence to support the relevance of this model has been discussed in detail by Schoelkopf *et al*. (2000a). These structures comprise cubic pores connected by cylindrical throats of chosen connectivity placed on a three-dimensional 10x10x10 position matrix. Previously, the network model has been used to simulate the void structure of porous media by fitting as closely as possible the simulated mercury intrusion curve of the model structure to that of the experimentally determined mercury intrusion curve of the actual sample. This procedure does not assume the traditional bundle of capillaries, but includes pore screening effects, such that the network properties and their influence on the intrusion are included. It was this feature of the modelling procedure that gave the successful correlation between imbibition modelling and real experimental structures (Schoelkopf *et al.*, 2000a). The parameters include pore size distribution, throat diameter distribution, porosity and connectivity.

Refined model structures of this type were used previously by Ridgway and Gane (2002) to simulate the absorption of a number of different fluids into a wide range of structures. Based on this practical experience, it was considered that the network model can be used as a 'predictor' tool rather than a simulator of existing experimental results. To illustrate this, structures that were generated, such that certain parameters could be isolated and their influence on the absorption behaviour of a fluid identified, were reported (Ridgway and Gane, 2002). It was shown how, keeping the porosity constant, structures can be represented in a number of different ways and that these structures have vastly different absorption behaviour. This finding confirms the inadequacy of the bundle of capillaries model and the need to introduce network complexity, as exemplified in these models. Reducing the value of the fluid density in the network simulation was also investigated to show where the transition

[1] Pore-Cor is a software program of the Environmental and Fluid Modelling Group, University of Plymouth, PL4 8AA, U.K.

occurs in the absorption behaviour from the linear t-dependent short timescale inertial Bosanquet regime (Bosanquet, 1923) to the $\sqrt{t}$ Lucas-Washburn viscous regime, following the procedure of Schoelkopf *et al.* (2000a). This is further discussed below when considering the imbibition algorithm used to model the imbibition.

In the work reported here, the results from imbibition modelling are compared with the actual experimental observations of absorption into real network structures. These experimental samples were specially constructed from constant mineralogy fine ground calcium carbonate having the same maintained surface chemistry (wetting energy and contact angle). The contact angle applicable is therefore considered constant. Its actual value is not relevant to the findings here as the relative results are important rather than the absolute. However, the contact angle for the relevant fluid was previously determined on a single crystal of the same calcite by applying dispersing agent in the wet state and measuring the contact angle using an optical microscope technique (Schoelkopf *et al.*, 2002). The range of applicability of the Lucas-Washburn equation (Lucas, 1918; Washburn, 1921) to describing experimental absorption is analysed. Imbibition studies were made by bringing each porous sample into contact with a supersource of liquid and the dynamic absorption was recorded gravimetrically.

Results from both modelling and experiment are shown to follow a long timescale macroscopic absorption rate depending approximately on the square root of time, but despite this macroscopic property they show a failure to scale according to the pore size parameter in the Lucas-Washburn equation even though the constants of surface energy, contact angle and fluid viscosity have been strictly maintained.

The analysis shown below illustrates the underlying effects of network structure complexity in determining the absorption dynamic and the probability level of pore filling within the region of the progressing wetting front as derived from the interial competition between individual interconnected pores.

THE PORE-COR NETWORK MODEL

Pore-Cor is a computer model that simulates the void-space structure of porous materials. It has been used to simulate the structures of a wide range of porous materials including sandstones (Matthews *et al.*, 1996), medicinal tablets (Ridgway *et al.*, 1997) and soil (Peat *et al.*, 2000).

The Unit Cell

The network model uses a unit cell with 1 000 cubic pores in a regular three dimensional 10x10x10 array, connected by up to 3 000 throats (which in this work are assumed to be cylindrical), depending on the defined connectivity, i.e. the average number of throats connected to each pore in the unit cell. Each pore is equally spaced from its neighbouring pores by the 'pore row spacing' Q, and each unit cell is a cube of side length 10 Q. There are periodic boundary conditions, which are applied serially during wetting, with each cell connected to another identical unit cell in each direction. When used to simulate actual samples, the pore- and throat-size distributions of the unit cell are optimised so that the simulated mercury percolation curve fits as closely as possible to the experimental mercury intrusion curve (Matthews *et al.*, 1995), corrected for mercury compression, penetrometer

expansion and sample compression (Gane *et al.*, 1996). The model accounts for pore screening by the smaller throat diameters. This feature breaks the constraints of the traditional bundle of parallel capillaries and introduces a greater relevance derivable from the original mercury intrusion curve. The distribution of throat sizes is log-linear and the actual number of each pore and throat size is characterised by the parameter 'throat skew'. The throat skew is the percentage number of throats of the smallest size and the linear distribution between the minimum and the maximum size pivots about its mid-point at 1%. The positions of the pores and throats are random, determined by a pseudo-random number generator. The throats are randomly positioned within the array and the pores are then generated to be the size of the largest throat entering them.

The Wetting Algorithm

An algorithm incorporating short timescale inertial retardation, which effects a slowing of entry into the larger pores and initiates a short-lived linear time dependence in the finer pores, together with the longer term viscous drag component typified in the Lucas-Washburn relation, was created using a solution of the Bosanquet equation (Bosanquet, 1923) in which momentum considerations, avoiding the discontinuity of initial $t = 0$ acceleration by averaging techniques, form the basis for a time decaying function of the second of Newton's laws of motion applying to the inertia of a column of fluid mass entering a pore, (Ridgway *et al.*, 2001). For water and thin mineral oils, (Schoelkopf *et al.*, 2000b), this occurs within the first ≤ 0.1 µm in a timescale of ~ 10 ns. Denser low viscosity fluids have a longer lasting inertial effect. More viscous fluids have a shorter-lived inertial effect.

The wetting algorithm is applied to the cylindrical throats only, such that they act as simple capillary elements. The dynamic of flow through each throat is determined by the Bosanquet equation with the boundary condition of mass flow continuity. The throats deliver liquid to their connected pore. The exiting throat(s) from that pore are allowed to undergo wetting and filling once the pore itself is full and provided they are not already filling from another connected full pore. The volume flow through the exiting throats is limited by the input flow to the pore that is acting as the reservoir for the throat wetting. In this way, the cubic pores do not contribute to the wetting but act simply as reservoirs for the onward wetting front acting through the connected throats. This simplification obviates the need to consider more complex wetting phenomena, such as side wall wetting, fingering, groove or wedge capillarity etc., all of which are of course present in real network structures. The aspect ratio of the throat-like features is an important parameter in the response to this wetting algorithm. The work of Sorbie *et al.* (1995) dealing with pore doublets is discussed in detail by Ridgway *et al.* (2002) and extended by them to the 3D interconnectivity provided by the network model.

The Synthesised Model Structures

The network model is used here to simulate a range of predefined structures in order to investigate the effects on the absorption of a fluid both in respect to the composition of the void space of the unit cell and in respect to the fluid density and viscosity. Recent modelling and experimental observations by Gane *et al.* (2000) and Schoelkopf *et al.* (2000b) have highlighted the possibility of developing rapid absorption properties with respect to water and low viscosity oils by concentrating the pore size distribution of thin layer porous media within the 0.05 to 0.1 µm region. This leads to a concentration of the otherwise

differentiating preferred pathway dynamic of absorption caused by inertial retardation of short timescale imbibition into larger pores. For this reason, a pore size distribution concentrated around 0.1 µm has been chosen to represent the majority of the simulations here, each lying around the expected pore-size transition point between inertial and viscous wetting for the fluids of interest.

(i) idealised monosized pore structures

The network model generates 100 different sized throats spread equally over a logarithmic axis between the minimum and maximum throat diameters. To illustrate the parameters, a number of monosized structures are first considered. By entering into the model almost identical settings for the minimum and maximum diameters, in fact with a narrow distribution of +/- 0.001 µm between the maximum and minimum, an effectively monosized pore structure is obtained. A series of differently sized 'monosized' distributions, constructed in this way, ranging from 0.01 µm to 5 µm was generated. An arbitrary connectivity value of 4 was initially used throughout, and a throat skew of 1 was adopted such that equal numbers of all possible logarithmically distributed throat sizes (in this case limited closely to monosize) were used to develop a fixed porosity of 50 %. As a result, the pore row spacing, Q, scales with the pore diameter increase, as shown in Table 1. An example of this type of structure is shown in Figure 1, (Ridgway and Gane, 2002).

Minimum diameter (µm)	Maximum diameter (µm)	Throat skew	Connectivity	Porosity, f (%)	Pore row spacing, Q (µm)
0.009	0.011	1	4	50	0.0154
0.019	0.021	1	4	50	0.0308
0.049	0.051	1	4	50	0.0769
0.099	0.101	1	4	50	0.1530
0.199	0.201	1	4	50	0.3070
0.499	0.501	1	4	50	0.7680
0.999	1.001	1	4	50	1.5300
1.999	2.001	1	4	50	3.0700
4.999	5.001	1	4	50	7.7400

Table 1 A variety of monosized pore structures, maintaining a constant porosity of 50 %.

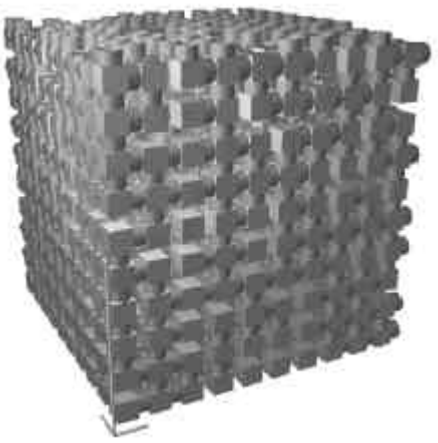

Figure 1 Network model unit cell of monosize 0.5 µm, unit cell size = 7.68 µm.

(ii) increasing the range of throat sizes around a common median

In a further step toward realistic natural porous samples, a range of pore sizes is now introduced. In the case of paper coatings (the main area of interest for the authors) this breadth of size distribution is an important parameter in balancing the optical properties of a coating layer with its printing properties (Gane, 2001a; Gane, 2001b). The size range within a model structure is here step-wise increased around the central median value of 0.1 µm (chosen, as discussed previously, because of its importance as the realistic decay point of the inertial imbibition effect for the typical fluid densities and viscosities used in printing). The unit cells here have been constructed such that their size, i.e. pore row spacing, Q, has been kept constant, keeping a constant number of throat entries per unit cross-sectional entry area. This is important so as not to confuse the absorption dynamic with a density function of accessible pore entry as the liquid is applied. This was effectively achieved by adjusting the porosity as the pore size range was varied. Again, the throat skew was set to 1 to generate an equal number of all the possible logarithmically distributed throat sizes within the desired limits. The network model parameters are shown in Table 2 and an example of a unit cell with a range of feature sizes is shown in Figure 2, (Ridgway and Gane, 2002).

Minimum diameter (µm)	Maximum diameter (µm)	Throat skew	Connectivity	Porosity, f (%)	Pore row spacing, Q (µm)
0.095	0.105	1	4	0.05	5.5
0.050	0.500	1	4	0.29	5.5
0.010	1.000	1	4	0.65	5.5
0.009	2.000	1	4	2.42	5.5
0.006	3.000	1	4	5.60	5.5
0.005	5.000	1	4	17.00	5.5

Table 2 Parameters used in the network model generations.

Figure 2 The network model unit cell with pore and throat size distribution 0.005 – 5.000 µm, unit cell size = 55 µm.

(iii) extending the range of throat size above and below a median, respectively

Two other size ranges are now investigated, one adding in features that are limited to being larger than 0.1 μm and the other adding in features that are limited to being smaller than 0.1 μm, once again each time keeping the pore row spacing constant so that the number of throat entries per unit area is constant. The network model parameters for these structures are shown in Table 3 and Table 4. The limit here is that a self-consistent pore row spacing within each set, i.e. one for increasing throat size and another for decreasing throat size, must be used. [A fuller range of unit cells can be seen in further detail in Ridgway and Gane (2002).]

Minimum diameter (μm)	Maximum diameter (μm)	Throat skew	Connectivity	Porosity, f (%)	Pore row spacing, Q (μm)
0.1	0.101	1	4	0.05	5.5
0.1	0.500	1	4	0.39	5.5
0.1	1.000	1	4	1.47	5.5
0.1	3.000	1	4	9.10	5.5
0.1	5.000	1	4	30.60	5.5

Table 3 The network model parameters for the structures extending ≥ 0.1 μm.

Minimum diameter (μm)	Maximum diameter (μm)	Throat skew	Connectivity	Porosity, f (%)	Pore row spacing, Q (μm)
0.099	0.1	1	4	99.0	0.1
0.050	0.1	1	4	77.0	0.1
0.010	0.1	1	4	46.5	0.1
0.005	0.1	1	4	39.4	0.1
0.002	0.1	1	4	32.7	0.1

Table 4 The network model parameters for structures extending ≤ 0.1 μm.

Imbibition

The simulated volume absorption curves as a function of time for all the above structures, results of which will be discussed below, were generated for this study initially using the fluid properties of water (surface energy, g = 0.07275 Nm^{-1}, contact angle, q = 0^o (the calcite is dispersed with a strongly hydrophilic polyacrylate), viscosity, h = 0.001 $kgm^{-1}s^{-1}$ and density, r = 998 kgm^{-3}). Selected changes in viscosity and density have also been investigated to illustrate their effects and to cover a broad spectrum of values of potentially relevant experimental fluids.

EXPERIMENTAL

Materials

Two commercially available dry powder products, both derived from natural calcium carbonate, ground under similar chemical conditions from the same Orgon, France, limestone source, were used, as reported by Schoelkopf *et al.* (2002). The grinding was made in a wet state at consistent solids content using a polyacrylate dispersing agent applied in proportion to the specific surface area of the final pigment size distribution and subsequently dried. The two size distributions of the respective products were chosen to be different in respect to the quantity of particles less than the 2 µm Stokesian equivalent hydraulic diameter, being 60 % w/w < 2 µm and 95 % w/w < 2 µm, defined as "coarse $CaCO_3$" and "fine $CaCO_3$", respectively. The mass cumulative particle size distribution curves of the two materials, as measured by sedimentation[2], are shown in Figure 3.

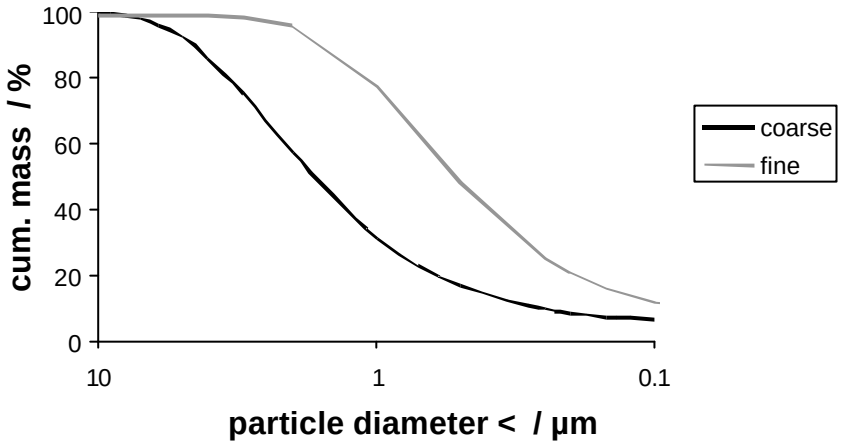

Figure 3 Particle size distributions of the coarse and fine $CaCO_3$ powders used for consolidation of porous tablets expressed as cumulative mass % less than an equivalent Stokesian diameter.

The bulk samples prepared for imbibition studies are cuboid blocks of each ground pigment, compacted over a range of pressures to form a series of well-defined porosities. The detailed method of powder compaction, applying pressures up to ~ 260 MPa in a steel die on an hydraulic press and subsequent sample grinding, is described more fully elsewhere (Gane *et al.*, 2000). The porosity range achievable with the coarse powder was found to be much broader (~ 20-40 %) than the range achievable with the fine pigment (~ 26-33 %), indicating the differences in initial packing characteristics and compressibility. The samples, being consolidated and therefore maintaining their integrity, did not require a sample vessel for the fluid imbibition experiments, thus eliminating uncertainties of fluid interactions between the sample and such a vessel.

To reduce artefacts caused by the wetting of their outer surfaces, the samples were coated with a thin barrier line of a silicone polymer[3] around the base of the vertical edges arising from the basal plane. The remainder of the outer planes were not coated to allow for the free

[2] Measurements made on a Sedigraph 5100
[3] Dow Corning P4-3117 conformal coating

movement of displaced air during liquid imbibition, and to minimise any interaction between the silicone and the absorbed liquid.

The experimental liquid used was a mineral oil[4] (aromatic free quality), as employed typically in the formulation of offset printing inks. The contact angle of oil/calcium carbonate, *q*, was assumed to be zero following the data of Chibowski *et al*. (1997), who have shown that aliphatic alkanes completely wet a number of mineral surfaces including calcium carbonate - this being the basis upon which alkanes were used to determine an effective pore radius. Additionally, this wetting behaviour was also confirmed by observing the complete spreading of an oil droplet on a dispersant pre-adsorbed macro-crystal surface of calcium carbonate. An oil viscosity of 0.0043 $kgm^{-1}s^{-1}$ was determined with a StressTech rheometer performing a small ramp of shear rates showing Newtonian behaviour. The surface tension was measured to be 0.0274 Nm^{-1} by the means of a Krüss Digital Tensiometer K10T. The density of 805 kgm^{-3} was given by the manufacturer. These values indicate that it can be assumed to be an alkane isomeric blend of around C_{16}.

Mercury Porosimetry

Each structure used for the experimentation was analysed independently with mercury porosimetry. A Micromeritics Autopore III mercury porosimeter was used to measure the intrusion characteristics of the samples. The maximum applied pressure of mercury was 414 MPa (60 000 psia), equivalent to a Laplace throat diameter of 0.004 µm. Small samples were used, each of around 1.5 g in weight. The equilibration time at each of the increasing applied pressures of mercury was set to 60 seconds. The mercury intrusion measurements were corrected for the compression of mercury, expansion of the glass sample chamber or 'penetrometer' and compressibility of the solid phase of the sample by use of the following equation (1) from Gane *et al*. (1996), as incorporated in the software Pore-Comp[5].

$$V_{\text{int}} = V_{\text{obs}} - dV_{\text{blank}} + \left[0.175 (V^1{}_{bulk}) \log_{10} \left(1 + \frac{P}{1820} \right) \right] - V^1{}_{bulk} (1 - \Phi^1) \left(1 - \exp \left[\frac{(P^1 - P)}{M_{\text{ss}}} \right] \right) \qquad (1)$$

where V_{int} is the volume of intrusion into the sample, V_{obs} the intruded mercury volume reading, dV_{blank} the change in the blank run volume reading, $V^1{}_{\text{bulk}}$ the sample bulk volume at atmospheric pressure, P the applied pressure, Φ^1 the porosity at atmospheric pressure, P^1 the atmospheric pressure and M_{ss} the bulk modulus of the solid sample. The volume of mercury intruded at the maximum pressure, once corrected for sample compression effects, can be used to calculate the porosity of the sample. For convenience, a representative (median intrusion) pore radius is defined as $r_{50} = d_{50}/2$, where d_{50} is the pore diameter, at which 50 % of the corrected mercury intrusion volume occurs.

Liquid Imbibition Methodology

The recording of the position of the liquid front within the sample by eye or camera is imprecise due to the fuzzy appearance of the wetting front. This is assumed to be due to the previously discussed suspected preferred pathway flow arising from the inertial competition between pores of different sizes at the wetting front.

[4] Haltermann PKWF 6/9 af

[5] Pore-Comp is a software program of the Environmental and Fluid Modelling Group, University of Plymouth PL4 8AA, U.K.

The rate of liquid mass uptake was measured instead gravimetrically using an automated microbalance, namely a PC-linked Mettler Toledo AT460 balance with a precision of 0.1 mg, capable of 2.7 measurements per second. A software program was developed (Schoelkopf *et al.*, 2000a) and improved further in the present work, interfacing with the balance for data sampling[6]. To provide a sufficiently slow and precise approach of the sample down to the liquid surface, a special sample holder was constructed - details of which are given elsewhere (Schoelkopf *et al.*, 2000a). All experimentation in this study was maintained under constant temperature conditions of 23.0 ±1.5°C. Experiments with five similar samples were shown to have a repeatability within ±0.96 % in absorption mass at 1 000 s (Schoelkopf *et al.*, 2000a).

ANALYSIS OF EXPERIMENTAL AND MODEL ABSORPTION RATES

The analysis performed here uses the methodology outlined by Schoelkopf *et al.* (2002) and is designed to investigate whether the Lucas-Washburn equation applies universally for porous network structures when the skeletal surface properties are held constant.

An equivalent hydraulic radius for an equivalent hydraulic capillary (ehc), which behaves in the same absorptive way as the structures, can be defined. It is possible to define an ehc based on apparent Darcy absorption distances into the structures as a function of time. The concept of Darcy length represents the filled length that would be present if the sample were modelled by a distribution of bundled straight capillaries given by the function of the geometric mean of their radii. If we were to derive an ehc of radius r_{ehcDarcy}, based on Darcy *length* ($V(t)/(Af)$), where V is the volume absorbed over a cross-section A in a sample having porosity f, as defined by Lucas-Washburn, it would follow

$$r_{\text{ehcDarcy}} = \left(\frac{V(t)}{Af} \right)^2 \frac{2h}{g_{\text{LV}} \cos q \; t} = \left(\frac{\mathrm{d}(V(t)/A)}{f \; \mathrm{d}\sqrt{t}} \right)^2 \frac{2h}{g_{\text{LV}} \cos q} \qquad (2)$$

where h is the fluid viscosity, g_{LV} is the fluid surface tension between the meniscus and the vapour phase (air), q is the contact angle between the advancing meniscus and the solid phase and t is the time. When the ehc is defined based on experimental *volume* uptake, as in the experiments here, the measurement is that of liquid mass uptake as a function of time into the porous compressed pigment tablets of defined porosities. The designed consistent surface chemistry of the skeletal pigments and fluid properties in this study result in a constant value for $g_{\text{LV}}\cos q$. Furthermore, the definition of an ehc is independent of fluid and surface energy properties, as the volume uptake is an experimental parameter which is effectively normalised by the interactional components in Eqn. 2. Modelling this equation using a range of fluids in model structures, therefore, results in a consistent value for the ehc for all fluids which can then be compared with experiments based on a single fluid.

It is shown experimentally that the rate of volume uptake approximates to a $\sqrt{t}$ relationship, as shown in Figure 4.

[6] Software available from the authors.

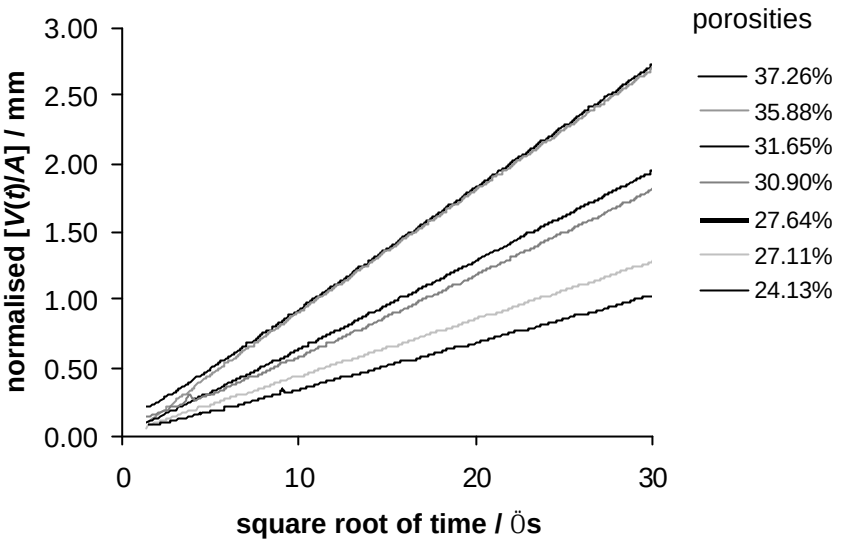

Figure 4 Absorption curves for increasing experimental porosities (from bottom to top, same order as in legend) normalised to $V(t=0)/A=0$ to remove wetting jump. Data shown are for the coarse $CaCO_3$ series.

The simulated absorption curves into the model structures also approximate to a $\sqrt{t}$ relationship, Figure 5 and Figure 6. In the case of the monosized structure the slight step at the beginning is a result of the first layer of throats filling. This phenomenon is discussed later.

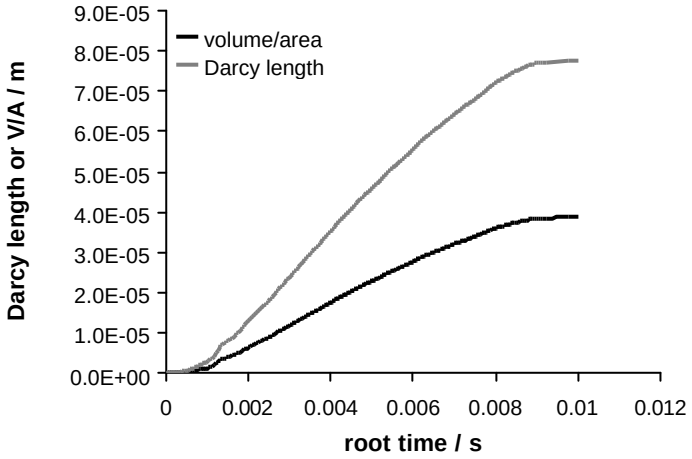

Figure 5 Simulated absorption curve for 5 µm monosized unit cell expressed as a Darcy length and in terms of volume/area.

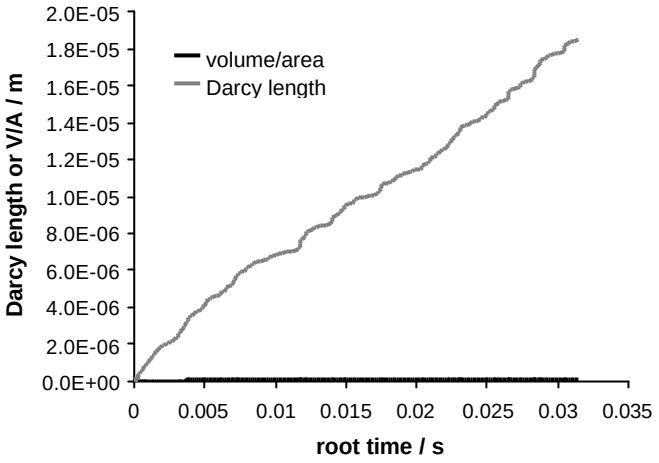

Figure 6 Simulated absorption curve for unit cell with size range 0.01 – 1.0 µm expressed as a Darcy length and in terms of volume/area.

Therefore, the absorption curves can be expressed as a linear relationship between $V(t)/A$ and $\sqrt{t}$, the gradient of which is

$$\frac{\mathrm{d}(V(t)/A)}{\mathrm{d}\sqrt{t}} = \frac{\mathrm{d}((m(t)/r)/A)}{\mathrm{d}\sqrt{t}} \tag{3}$$

where $m(t)$ is the mass uptake at time t, as defined by a volume $V(t)$ of fluid of density r. The data are normalised to the cross-sectional area of the sample, A, such that the data become $V(t)/A$, the volume absorbed per unit cross-sectional area of the sample. The gradient can be obtained directly from the plotted data by a linear regression analysis.

If we assume at first the universality of the Lucas-Washburn equation, the volume uptake per unit cross-sectional area of the sample should be expressed in terms of the basic interactional parameters between fluid and the solid surface making up the boundaries of the pores as

$$V(t)/A = \frac{1}{A} p\, r_{ehc}^2 \sqrt{\frac{r_{\mathrm{ehc}} g_{\mathrm{LV}} \cos q\ t}{2h}} \tag{4}$$

formed by balancing the Laplace pressure across a curved meniscus with the Poiseuille resistive laminar flow in the circular capillary, and letting the volume uptake per unit area equal the volume filled into our equivalent capillary of radius r_{ehc}, which represents that unit area. This definition no longer relates directly to the porosity of the sample and the experimental incompatibility with the previously defined Darcy ehc, r_{ehcDarcy}, becomes a natural consequence.

From Eqn. 4 the r_{ehc} is derived for each structure separately by comparing the experimental uptake gradients with the assumed parameters of the Lucas-Washburn equation acting over unit area, such that

$$\frac{\mathrm{d}(V(t)/A)}{\mathrm{d}\sqrt{t}} = \frac{p\, r_{ehc}^2}{A}\sqrt{\frac{r_{\mathrm{ehc}} g_{\mathrm{LV}} \cos q}{2h}} \tag{5}$$

from which r_{ehc} can be isolated as

$$r_{\mathrm{ehc}} = \sqrt[5]{\left(\frac{\mathrm{d}(V(t)/A)}{\mathrm{d}\sqrt{t}}\right)^2\left(\frac{A}{p}\right)^2\frac{2h}{g_{\mathrm{LV}}\cos q}} \quad = \quad \sqrt[5]{\left(\frac{\mathrm{d}V(t)}{\mathrm{d}\sqrt{t}}\right)^2\frac{2h}{p^2 g_{\mathrm{LV}}\cos q}} \tag{6}$$

Comparing this volume-based r_{ehc} value with the value we obtained for r_{ehcDarcy} based on Darcy length (Eqn.2), we see that

$$r_{ehc}^5 = r_{\mathrm{ehcDarcy}}\left(\frac{Af}{p}\right)^2 \tag{7}$$

This relationship only holds experimentally if the imbibition rate follows an exact $\sqrt{t}$ relationship over all time. If this is not the case then the manipulation of both the exponent and the inclusion of porosity weight the radii away from the equivalent independently derived values and reinforces the influence of the absorption behaviour at longer times and provides a modified value for r_{ehc} which we define as r'_{ehc}. In our experiments and modelling, the longer times are more consistently $\sqrt{t}$ related and so, as shown below, the use of Eqn. 7 can be considered as a means of extracting the interactional properties of a porous medium during wicking even though the short timescale absorption may not be directly Lucas-Washburn in nature.

EFFECT OF STRUCTURE AND DISCUSSION

The Network Models

(i) idealised monosized pore structures

As defined above, the absorption curves corresponding to the predetermined network model structures can be plotted either as Darcy length or as volume per unit area uptake, against square root of time. The gradients from these curves are then used to calculate r_{ehcDarcy} and r_{ehc}, respectively, for each structure and each set of fluid parameters. Both higher and lower density and viscosity values were investigated with the monosized pore and throat size distribution structures. A plot of r_{ehcDarcy} against the simulated mercury intrusion r_{50} for these structures is shown in Figure 7.

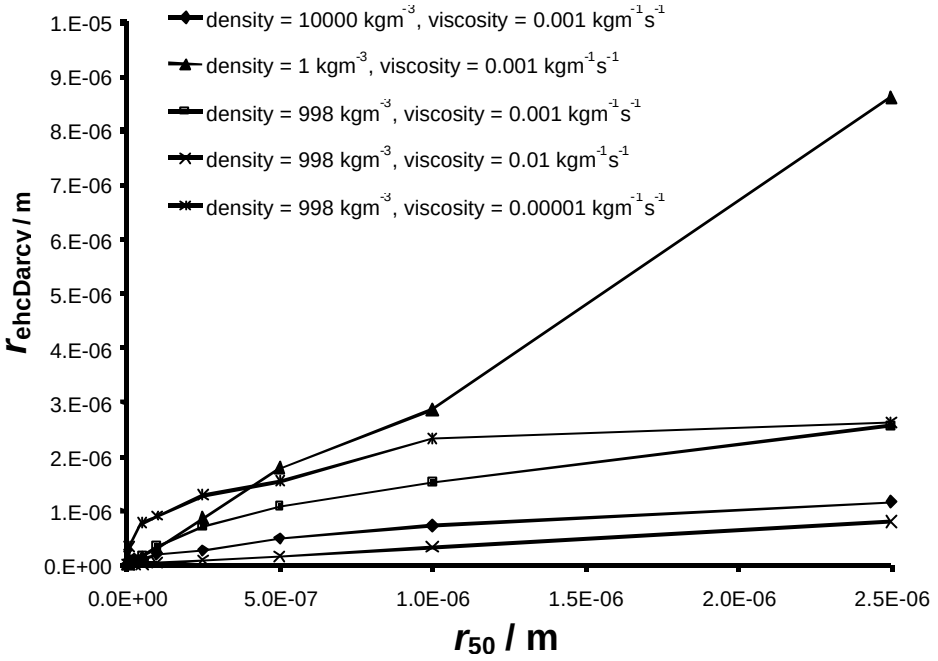

Figure 7 r_{ehcDarcy} values against the r_{50} values for a series of increasing monosize network model unit cells.

Taking each curve separately and fitting a linear trendline it can be seen that the linear relationship between r_{ehcDarcy} and r_{50} only holds true for low density or high viscosity. This linear relationship corresponds to the prediction of Lucas-Washburn. In other cases, high density and/or very low viscosity, the effect of inertia in the model breaks this linearity. This is an important feature of inertial wetting within a network structure. We can no longer assume that the impact of inertia is over in the first few nanoseconds of absorption as is the case for a single capillary or bundle of capillaries. The inertial effect acts every time the fluid is accelerated or decelerated within the changing features of a permeable structure. These effects are then tempered by the viscous drag behind the wetting front. However, with a broad range of reservoirs which form the feed for the wetting front as it progresses, the continuing differentiation between fine pores (preferred) and large pores means that the volume flow rate in the bulk of the sample is enough to feed the inertial differentiation adaequately at the wetting front itself, i.e. *inertia is continuously relevant at the wetting front*.

The equivalent volume-based capillary radius, r_{ehc}, can also be calculated from a plot of volume uptake per unit area against time, Eqn. 6. Figure 8 shows r_{ehc} plotted against r_{50} for the monosized unit cells.

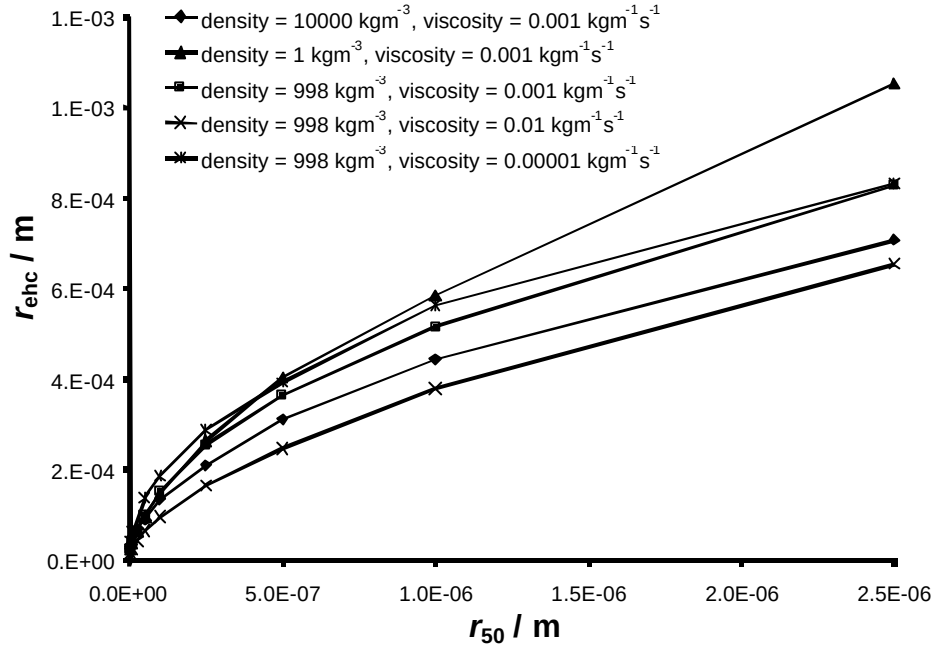

Figure 8 Volume-based r_{ehc} plotted against r_{50} increasing pore size in the monosized network model unit cells.

Using Eqn. 7 it is also possible to calculate the analytically-expected r'_{ehc} from the $r_{ehcDarcy}$ values. These values are shown in Figure 9.

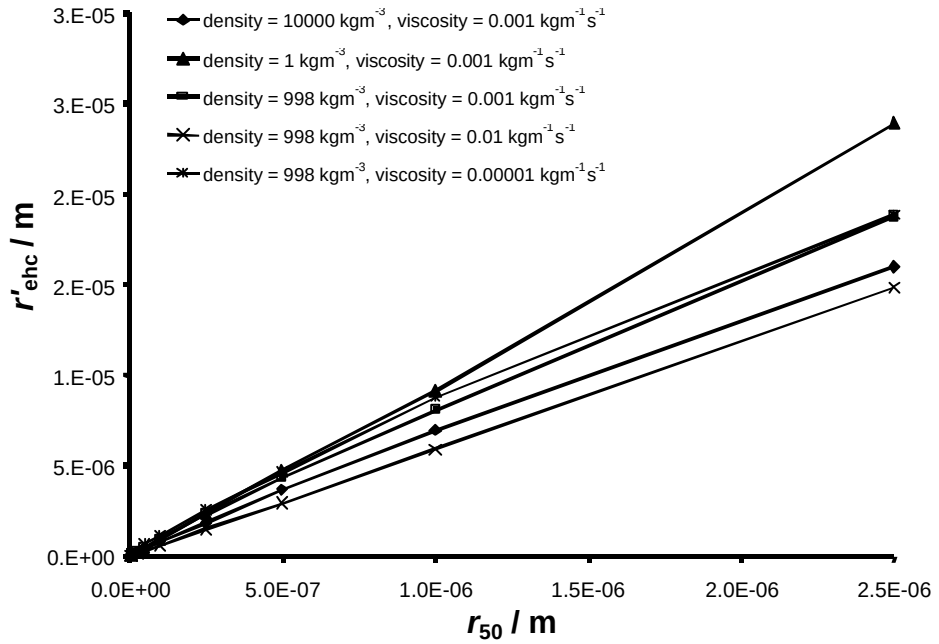

Figure 9 Volume-based r'_{ehc} as calculated from $r_{ehcDarcy}$ (Eqn. 7) plotted against r_{50} for increasing pore size in the monosized network model unit cells.

There are some points of interest which should be taken into account when considering the analysis of the model absorption data:

1. As we see in Figure 8 and Figure 9, there is an incompatibility between the calculated, r'_{ehc}, and the directly determined values for r_{ehc}. This relates to deviation from purely $\sqrt{t}$

behaviour over some part(s) of the absorption curve and the effect of porosity on weighting this deviation. The network model structures have an artefact which interferes with a straightforward Lucas-Washburn response at short times. This is because initial imbibition is only in the top layer of throats and in the $-z$ direction. The top surface of the unit cell is not really a cross-section of the structure as there are no xy imbibition possibilities at time t=0. This distorts the absorption-time data at the origin and makes it difficult to define a given parameter against $\sqrt{t}$ gradient that is relevant for all times.

2. A second factor is that even after longer times the absorption is not exactly linear with respect to $\sqrt{t}$ for all the fluid combinations, although the deviation in some cases is small. This means that the definition of the $\sqrt{t}$ absorption gradient is strongly dependent on the weighting of the chosen parameter given by the porosity factor (see Eqn. 7 for example). The higher the porosity, the more the longer time region becomes effectively weighted disproportionately when determining the $\sqrt{t}$ gradient for absorption volume compared with Darcy length. The direct mathematical regeneration of r'_{ehc} from the r_{ehcDarcy} definition is therefore not reproducible when cross-referencing the terms generated directly from the data. However, the trends are reproducible.

These factors are an indication in themselves of deviation from Lucas-Washburn intrinsic to network structures, not simply because they are models here but because the acceleration of fluid within interconnecting networks should always be considered. [Further complexities of wetting in real structures also introduce other means for accelerating fluids]. These deviations, when seen experimentally, are traditionally often accounted for by introducing arbitrary structure parameters, such as tortuosity. In the case of the model structures such arbitrariness can be avoided. Nonetheless, the regeneration of r'_{ehc} via these weighting factors can provide a useful tool for deriving the interactional properties by forcing the absorption into an experimentally relevant $\sqrt{t}$ regime - this will be discussed further later.

(ii) broadening pore size distributions

By using fluids of different density whilst keeping viscosity constant (0.001 $\mathrm{kgm^{-1}s^{-1}}$), the imbibition was modelled in structures with broadening polydispersity. Figure 10 shows the results for the directly determined r_{ehcDarcy} as plotted against the simulated r_{50}.

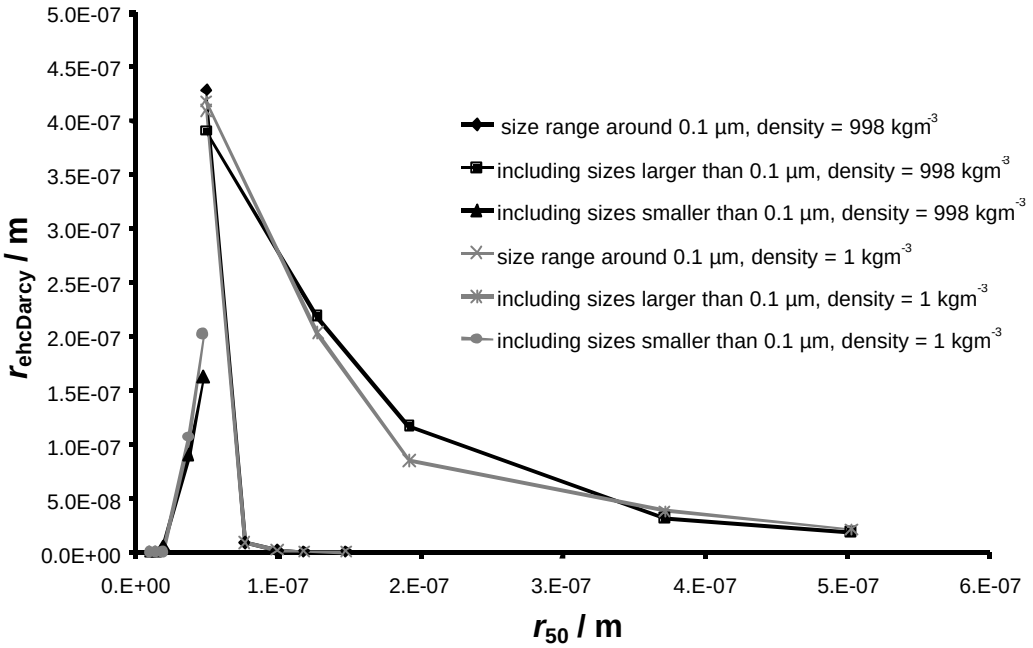

Figure 10 $r_{ehcDarcy}$ (Eqn. 2) plotted against the simulated r_{50} values for three series of model structures with increasing polydispersity using high and low fluid density values.

When features larger than 0.1 µm are progressively introduced into the model structure then the $r_{ehcDarcy}$ decreases as the r_{50} increases, this is the opposite of the Lucas-Washburn prediction which states that as larger features are included so the $r_{ehcDarcy}$ should get larger. This demonstrates mainly the effect of porosity which is apparently not catered for adequately by Eqn. 2. As the porosity increases, so the absorbed volume increases but not as fast as necessary to increase the apparent Darcy length of absorption, i.e. the classical equation ignores the impact of networks. Therefore, the $r_{ehcDarcy}$ apparently decreases as the pore size increases above 0.1 µm.

Similarly, as pore size decreases below 0.1 µm, the Darcy length of permeation also decreases again despite the increase in porosity. However, in this case, when features smaller than 0.1 µm are progressively included in the unit cells, the $r_{ehcDarcy}$ decreasing with decreasing r_{50} is consistent with Lucas-Washburn. This is logical because the resistance of the increasing number of finest pores in the bulk of the sample behind the wetting front quickly turns to viscous Poiseuille behaviour.

As the polydispersity broadens around 0.1 µm an even more dramatic effect is seen as the structure delivers low resistance in the large pores and high resistance in the finest pores. The greatest driving force in the structure for wetting, however, is concentrated in the finest pores. This leads to dependence on volume flow resistance through the fine pores, such that adequate flow is permitted by the large pores only which must be connected adequately to the finest pores if the greatest absorption depth is to be realised. Clearly, therefore, the optimal pore size concentration at 0.1 µm promotes the farthest apparent Darcy permeation into the sample. For a given set of fluid parameters, the greatest apparent permeation depth occurs in monosize structures.

Similar effects were seen experimentally by Gane *et al*. (2000) in which observed absorption penetration depth into compressed tablet structures after contact with fixed volume droplets showed a maximum absorption depth at a porosity of 24-26 %. From this work it would

suggest that this porosity corresponded to the minimum in polydispersity within the tablet series. Retrospective study of the pore size distribution of the samples does indeed confirm this hypothesis, as can be seen by the steeper experimental mercury intrusion curves around the critical porosity in Figure 11.

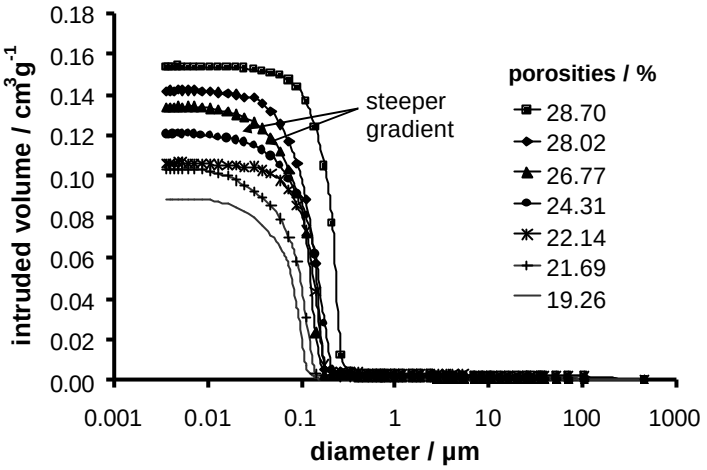

Figure 11 Experimental mercury intrusion curves for samples used in fixed volume droplet penetration experiments (Gane *et al.*, 2000).

The volume-based equivalent capillary radii, r_{ehc}, for the model unit cells with the various pore size ranges are once again calculated from the plots of volume uptake per unit area against $\sqrt{t}$, Eqn. 6. The respective r_{ehc} values are plotted against simulated r_{50}, as shown in Figure 12.

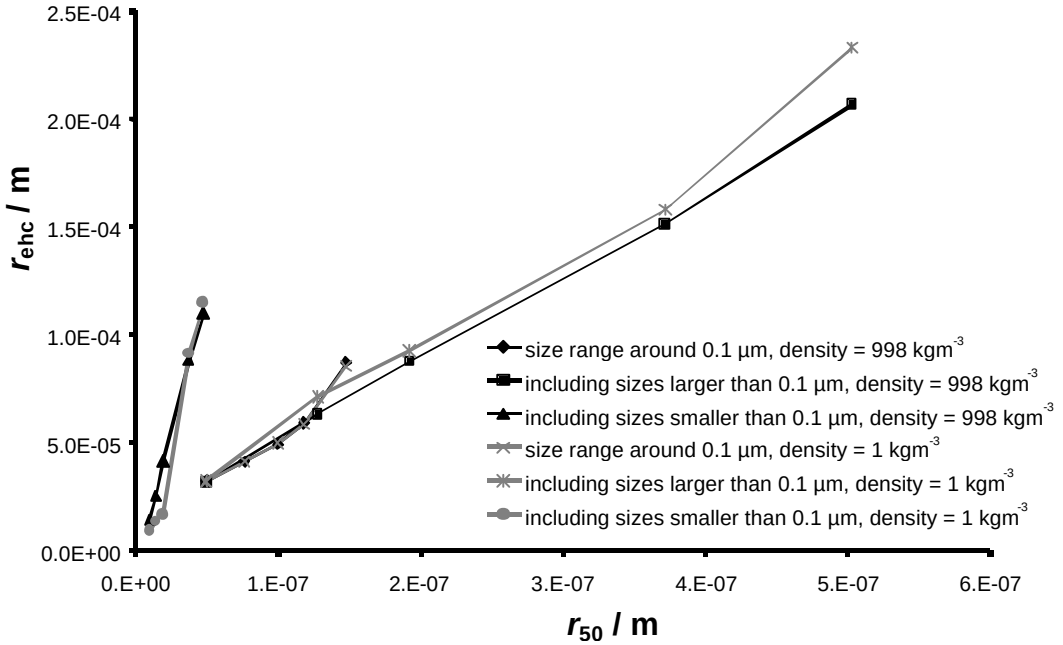

Figure 12 Volume-based r_{ehc} plotted against the simulated r_{50} values for three series of model structures with broadening size ranges with high and low fluid density values, viscosity = 0.001 $kgm^{-1}s^{-1}$.

In this case (Figure 12) we see a linear set of correlations between the volume-based r_{ehc} and r_{50} with expected group correlations applying within each pore size range, i.e. those including pores greater than 0.1 µm and those including pores less than 0.1 µm forming two separate groups.

Using Eqn. 7 it is also possible to calculate r'_{ehc} from the $r_{ehcDarcy}$ values. These values are shown in Figure 13.

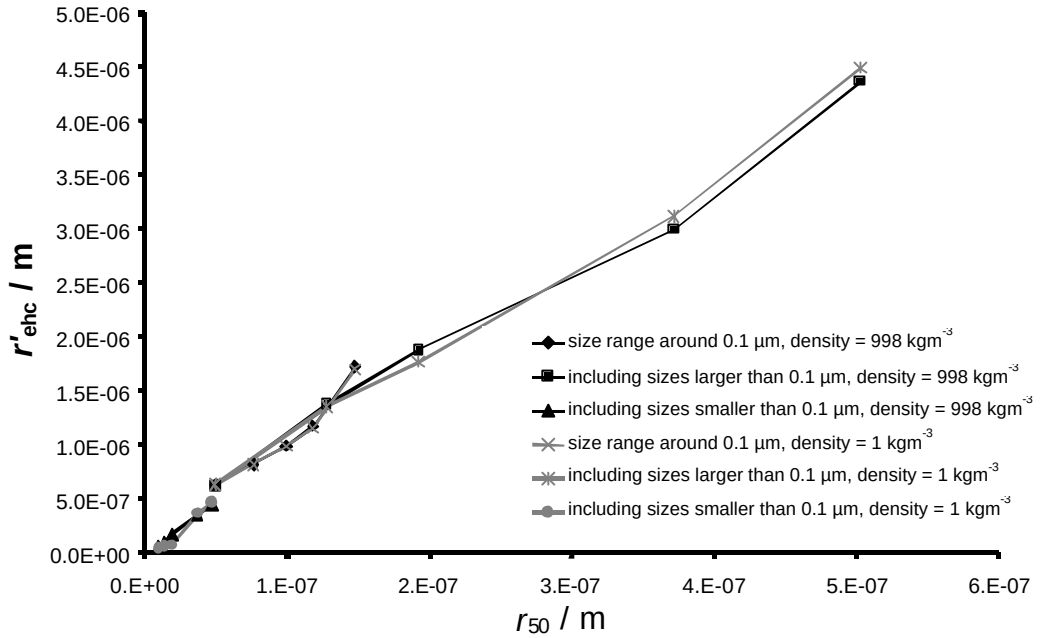

Figure 13 Derived r'_{ehc} (calculated from $r_{ehcDarcy}$, Eqn.7) plotted against r_{50} for three series of model structures with broadening size ranges with high and low fluid density values, viscosity = 0.001 $kgm^{-1}s^{-1}$.

These plots (Figure 13) show that the definition of r'_{ehc} for a model structure is potentially much more easily correlated experimentally with respect to measured pore size. They show, respectively, a monotonic increase in calculated r'_{ehc} as the simulated r_{50} increases when porosity is used to scale the Darcy-defined $r_{ehcDarcy}$ (Eqn. 7), compared with the two groups of relationships when calculated directly from simulated volume uptake rate (Figure 13 compared to Figure12). This comparison shows the strong dependency of volume absorption rate within these size ranges on the nature of the porosity of the sample and not on the actual pore size or simple porosity figure as would have been predicted by the simplistic application of Lucas-Washburn in terms of a Darcy permeation length or an experimentally volume-derived r_{ehc}. Porosity forms the cross-correlation between the two groups of samples and this correlation gives the first indication that the properties of a network can combine through its complexity of structure (connectivity, size distribution etc.) in determining the absorption dynamic consistently over a range of porosities, whereas definitions of structures by the simplistic parameters of pore size distribution and porosity do not. This condenses the argument to the point where we predict that permeability is an extra controlling parameter and is not predictable from the classical capillary bundle but needs the complexity of a network.

Comparison with experiment

Experimentally, the gradient of uptake volume as a function of $\sqrt{t}$ also follows an approximate linear relationship with porosity and confirms that this parameter describes typically the absorption dynamic of samples within this size range, both coarse and fine, (Figure 14). As the $\sqrt{t}$ relationship holds over the complete observation time for the experimental samples, r_{ehc} is seen to be equivalent to r'_{ehc}.

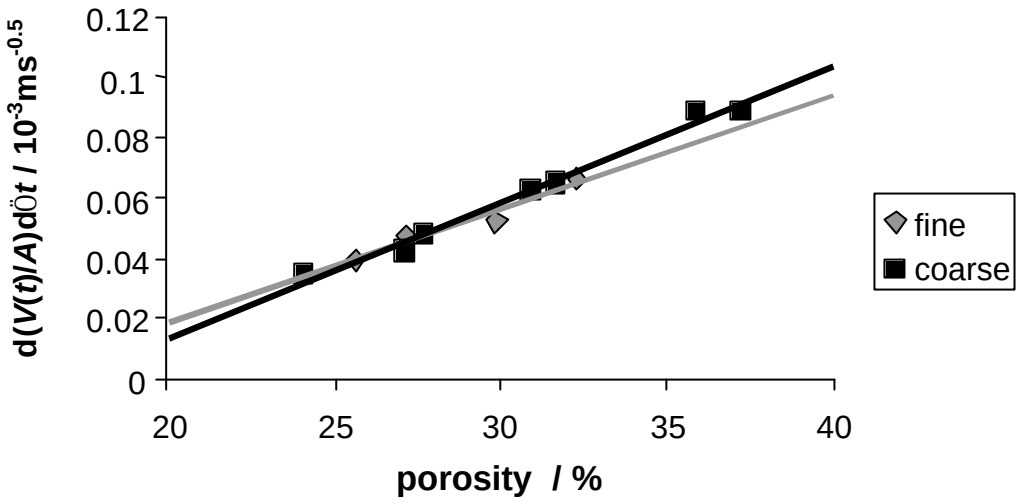

Figure 14 Both experimental structure series, differing in pore size distribution only, show similar volume rate absorption as a function of porosity.

The measured r_{50} values for these structures do not fall on the same trend between pigments as a function of porosity, as shown in Figure 15. This could also be seen with the modelled structures where fine and coarse structures are simulated, Figure 16. In both the experimental and simulation results, the coarse structures have a steeper gradient for r_{ehc} against r_{50}, and naturally larger r_{50} values, compared with the fine structures. If we compare the experimental observations with those according to Lucas-Washburn as functions of mercury porosimetry measured porosity, f_{Hg}, and pore size, r_{50}, we see that r_{ehc} scales with porosity, Figure 17, but does not scale between the two pigments as a function of pore size, Figure 18. These trends can again be seen with the simulation data in the models for the fine and coarse structures as shown in Figure 19 in comparable parameters and previously shown in Figure 13. Since the volume absorption dynamic was shown experimentally to be dependent strongly on porosity, and since all the Lucas-Washburn interactional parameters have been kept constant in these experiments, it must be assumed that the Lucas-Washburn equation for volume uptake based solely on pore size does not hold true for differing pore size distributions (and/or connectivity) in a network structure. The experimental evidence now supports the simulation plots qualitatively.

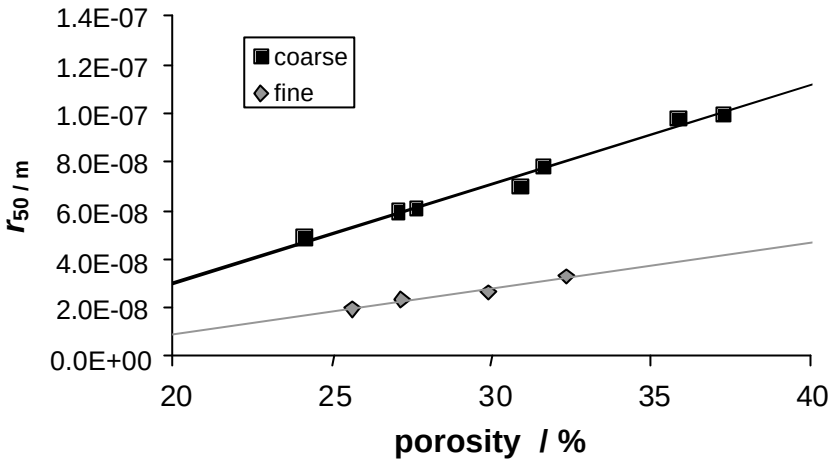

Figure 15 The measured r_{50} of the experimental structures as a function of porosity for the two different skeletal particle size distributions.

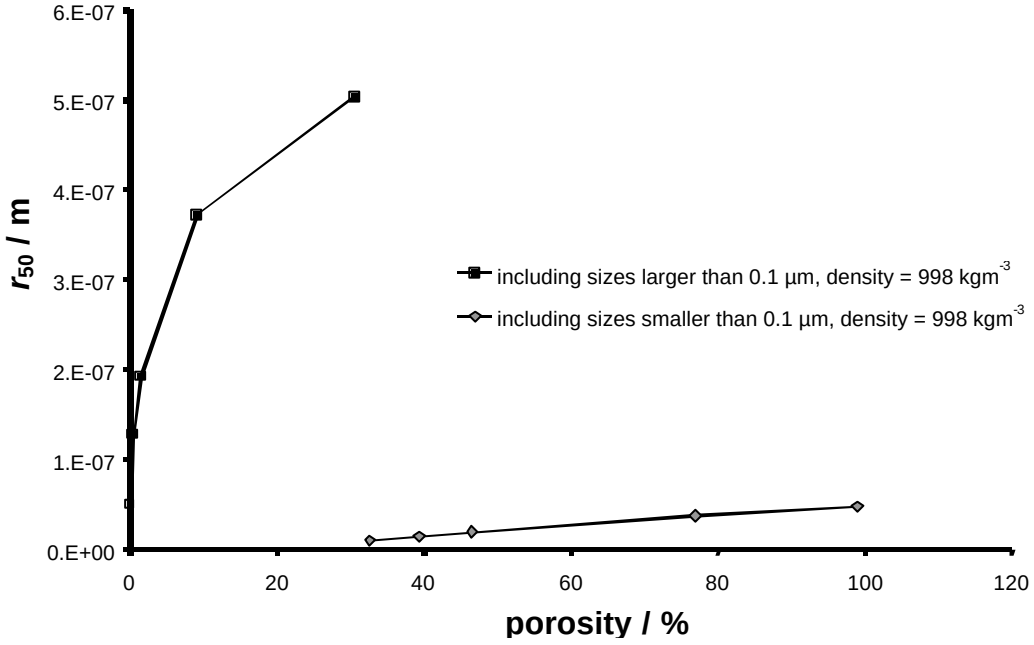

Figure16 Synthesized r_{50} from model structures as a function of porosity when introducing fine and coarse void size distributions.

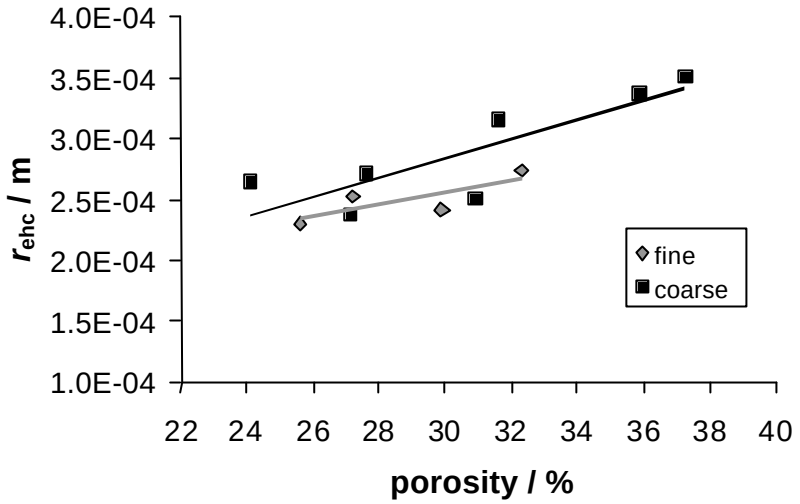

Figure 17 Volume-based r_{ehc} determined as a function of porosity shows quite similar behaviour for the two experimental structure series, despite each differing from one another in pore size distribution.

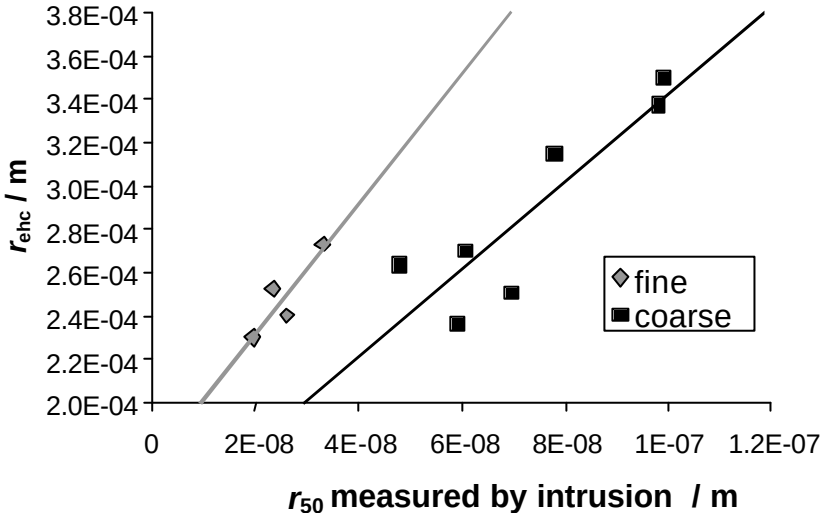

Figure 18 Volume-based r_{ehc} as a function of r_{50}. Note that there is no direct scaling across the two experimental structure series.

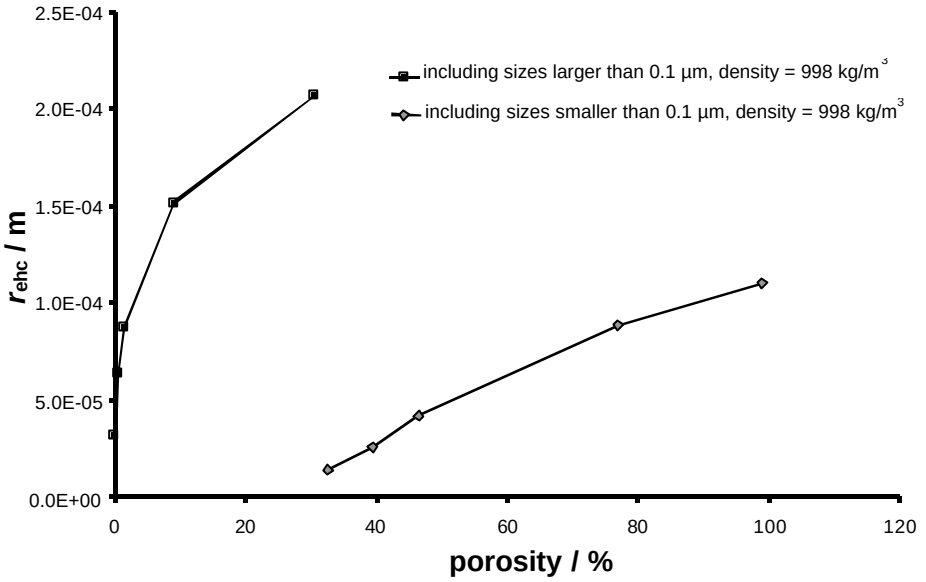

Figure 19 Volume-based r_{ehc} also fails to scale as a function of porosity for the coarse and fine synthesized void size distributions.

From all these plots it is seen that the scaling between an ehc, derived from data directly interpreted in terms of either a Darcy length or a volume uptake, and the measured pore size dimension breaks down, but that scaling with porosity is manifest within each structure group. By weighting the data in respect to porosity, by deriving a Darcy equivalent capillary radius from the volume-derived ehc, we obtain correlation between the equivalent capillary and the measured r_{50}. This behaviour of the experimental samples mirrors that predicted earlier for the models.

DETERMINING INTERACTIONAL AND STRUCTURAL PARAMETERS

Traditionally, it is notoriously difficult to determine the interactional properties $g_{LV}\cos q$ by wicking experiments due to the complications introduced by departure from Lucas-Washburn. This departure is now shown in part to be due to the effects of differing structural parameters such as connectivity and pore size distribution. Frequently, the best approximations deal with "apparent" values which can vary from sample to sample even though no rationale can be found for the deviation, or are compensated for by structural parameters such as the tortuosity factor.

The effect of connectivity in the model structures used here was studied. By using the monosize 5 µm unit cell it is possible to isolate the parameter of connectivity from the effects of pore size distribution. The connectivity was reduced stepwise from 6 to 2, adjusting the porosity such that the pore row spacing was kept constant. This resulted in the unit cells with higher connectivity having higher porosity values. By thus adjusting connectivity, the magnitude of the derived r'_{ehc}, using Eqn. 7, and the simulated r_{50} can be brought into agreement. This procedure can be represented as connectivity plotted against the ratio $b = r'_{ehc}/r_{50}$, Figure 20, such that a given value of b in monosized structures indicates the existence of a certain derivable connectivity. Conversely, a monosized structure of known connectivity can be used to determine $g_{LV}\cos q$ via a derived value for b.

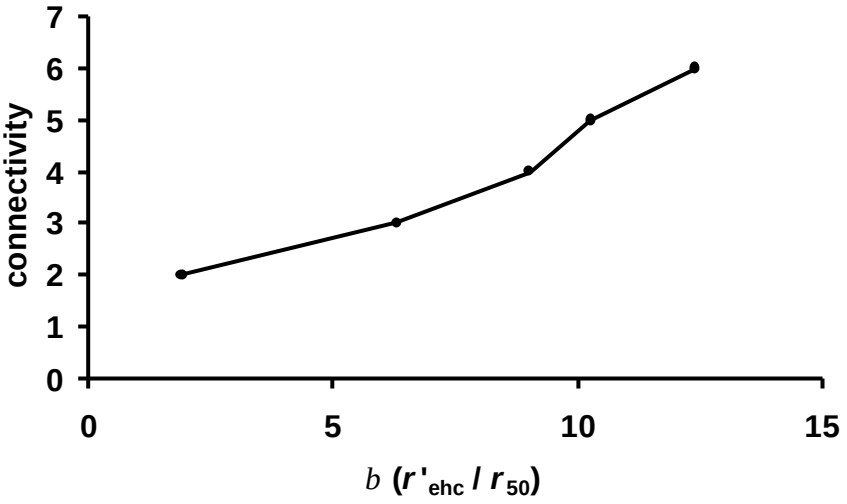

Figure 20 Connectivity for 0.5 µm model monosize structure plotted against the ratio $b = r'_{ehc}/r_{50}$

Basing the analysis on simplistic model structures clearly has the benefit of allowing one or more parameters to be isolated individually which provides the modeller with a foundation for understanding more complex networks. In more realistic structures, the factor b becomes a combined function of connectivity, tortuosity, pore size distribution and ultimately pore shape and pore shape distribution over the size range within the sample. The definition of our introduced parameter b, therefore, can be conveniently described as a network structure "complexity" parameter. Essentially this is a network descriptor and combines with the parameters of surface energy and porosity to determine the absorption behaviour of the structure.

As was seen for the earlier published experimental structures (Figure 11) (Gane *et al.*, 2000), the steeper the pore size distribution as defined by mercury porosimetry, i.e. the more monosize, the further the penetration front appeared within the sample for a given volume uptake and porosity. Such a structure has a relatively low newly-defined complexity parameter b. Similarly, the two experimental structures investigated here have different ratios of $b = r'_{ehc}/r_{50}$ with the finer carbonate showing the higher complexity.

The novel value of such a complexity descriptor is that it can potentially describe the degree of filling of a given network in respect to the advance of the wetting front. For example, the finer carbonate structure can be expected to have filled more completely per unit depth of penetration than the coarser carbonate, otherwise the function of absorption rate as dependent only on porosity for both samples individually would not have held. The mechanism for preferred pathway filling is therefore an apparent function of this descriptor within the types of structure investigated here.

CONCLUSIONS

Comparison of network model structures and experimentally observed absorption into structures with the same surface chemistry and morphological features shows qualitative agreement over a wide range of pore sizes and pore size distributions. The knowledge of the exact pore and throat dimensions in the network model (Pore-Cor) structures enables a clear

definition of absorption behaviour as a function of both pore size and porosity. Mercury porosimetry of experimental samples provides both pore size and porosity data for realistic porous media. At long timescales, absorption follows approximately, but not exactly, a $\sqrt{t}$ behaviour. At short timescales in the model systems there are deviations. The experimental absorption cannot be measured at such short timescales.

Scaling between the Lucas-Washburn-defined parameter of equivalent hydraulic radius and pore size for experimental samples and model structures of differing pore size and pore size distribution fails in both cases. Correlation is only brought into agreement when the porosity is included as a weighting factor, such that porosity cannot be assumed itself to be the controlling parameter. A correlation between measured pore size and porosity is not a prerequisite for this behaviour even when porosity is seen as the main controlling factor in a network structure.

A methodology is outlined whereby the sample properties are described by a network descriptor which expresses the complexity of the structure. This descriptor, b, is formed by the ratio of the volume-defined equivalent hydraulic radius, derived analytically from the porosity weighted Darcy permeation equivalent hydraulic radius under Lucas-Washburn conditions, and the measured 50 % mercury intrusion pore radius. This descriptor is suggested by modelling using an imbibition algorithm including inertial effects throughout the network to provide a prediction of the degree of filling of a porous network immediately behind the observed wetting front and can be used to predict the degree of preferred pathway differentiation during permeation which can lead to unfilled pores during the absorption dynamic. For structures containing fine pores which act within the inertial wetting regime (~ 0.1 µm diameter for fluids such as water and alkanes) the higher the value for b, the greater is the complexity of the structure and the fewer are the possible unfilled pores. This effectively means that highly complex fine structures with broad pore size distributions have a fast filling at short times despite their fine pore size and that the sample quickly saturates. Such highly complex structures represent well the fine pigmented layers found in paper coatings. More monosize pore structures result in greater permeation depth but with more unfilled pore volume.

REFERENCES

1. Batten,G.L.: 1984, Liquid imbibition in capillaries and packed beds, *Journal of Colloid and Interface Science* **102,** 513-518.

2. Bell,J.M. and Cameron,F.K.: 1906, The Flow of Liquids Through Capillary Spaces, *Journal Of Physical Chemistry* **10,** 658-674.

3. Bosanquet,C.H.: 1923, On the flow of liquids into capillary tubes, *Philosophical Magazine, Series 6* **45,** 525-531.

4. Chibowski,E. and Holysz,L.: 1997, On the use of Washburn's equation for contact angle determination, *Journal of Adhesion Science and Technology* 1289-1301.

5. Dube,M., Rost,M., and Alava,M.: 2000, Conserved dynamics and interface roughening in spontaneous imbibition: A critical review, *The European Physics Journal B* **15,** 691-699.

6. Einset,E.O.: 1996, Capillary infiltration rates into porous media with applications to Silcomp processing, *Journal of American Ceramic Society* **79,** 333-338.

7. Fisher,L.R. and Lark,P.D.: 1979, An experimental study of the Washburn equation for liquid flow in very fine capillaries, *Journal of Colloid and Interface Science* **69,** 486-492.

8. Gane,P.A.C.: 2001a, Mineral Pigments for Paper: Structure, Function and Development Potential (Part I), *Wochenblatt für Papierfabrikation* 110-116.

9. Gane,P.A.C.: 2001b, Mineral Pigments for Paper: Structure, Function and Development Potential (Part II), *Wochenblatt für Papierfabrikation* 176-179.

10. Gane,P.A.C., Kettle,J.P., Matthews,G.P., and Ridgway,C.J.: 1996, Void Space Structure of Compressible Polymer Spheres and Consolidated Calcium Carbonate Paper-Coating Formulations, *Industrial and Engineering Chemistry Research* **35,** 1753-1764.

11. Gane,P.A.C., Schoelkopf,J., Spielmann,D.C., Matthews,G.P., and Ridgway,C.J.: 2000, Fluid transport into porous coating structures: some novel findings, *Tappi Journal* **83,** 77-78.

12. Ichikawa,N. and Satoda,Y.: 1994, Interface dynamics of capillary flow in a tube under negligible gravity condition, *Journal of Colloid and Interface Science* **162,** 350-355.

13. LeGrand,E.J. and Rense,W.A.: 1945, Data on rate of caillary rise, *Journal of Applied Physics* **16,** 843-847.

14. Letelier,M.F. and Leutheusser,H.J.: 1979, Refined mathematical analysis of the capillary penetration problem, *Journal of Colloid and Interface Science* **72,** 465-470.

15. Levine S, Lowndes J, Watson,E.J., and Neale,G.: 1980, A theory of capillary rise of a liquid in a vertical cylindrical tube and in a parallel-plate channel, *Journal of Colloid and Interface Science* **73,** 136-151.

16. Levine,S., Reed,P., Watson,E.J., and Neale,G.: 1976, *A theory of the rate of rise of a liquid in a capillary*, Academic Press, New York.

17. Li,Z., Giese,R.F., van Oss,C.J., Kerch,H.M., and Burdette,H.E.: 1994, Wicking technique for determination of pore size in ceramic materials, *Journal of American Ceramic Society* **77,** 2220-2222.

18. Lucas,R.: 1918, Ueber das zeitgesetz des kapillaren aufstiegs von fluessigkeiten, *Kolloid Zeitschrift* **23,** 15-22.

19. Marmur,A. and Cohen,R.D.: 1997, Characterization of porous media by the kinetics of liquid penetration: the vertical capillaries model, *Journal of Colloid and Interface Science* **189,** 299-304.

20. Martic,G., Gentner,F., Seveno,D., Coulon,D., and DeConinck,J.: 2000, The Washburn equation at the microscopic scale, *6th International Symposium on Evaluation of Reservoir Wettability and Its Effect on Oil Recovery*, Soccoro, Mexico.

21. Matthews,G.P., Ridgway,C.J., and Small,J.S.: 1996, Modelling of simulated clay precipitation within reservoir sandstones, *Marine and Petroleum Geology* **13,** 581-589.

22. Matthews,G.P., Ridgway,C.J., and Spearing,M.C.: 1995, Void Space Modeling of Mercury Intrusion Hysteresis in Sandstone, Paper Coating, and Other Porous Media, *Journal of Colloid and Interface Science* **171,** 8-27.

23. Moshinskii,A.I.: 1997, Consideration of inertial force in capillary rise of a Newtonian liquid in a cylindrical tube, *Colloid Journal* **59,** 62-67.

24. Ostwald,W.: 1908, *Kolloid Zeitschrift* **Suppl. Heft II**.

25. Peat,D.M.W., Matthews,G.P., Worsfold,P.J., and Jarvis,S.C.: 2000, Simulation of water retention and hydraulic conductivity in soil using a three-dimensional network, *European Journal of Soil Science* **51,** 65-79.

26. Quere,D.: 1997, Inertial capillarity, *Europhysics Letters* **39,** 533-538.

27. Rideal,E.K.: 1922, On the flow of liquids under capillary pressure, *Phil.Mag.Series 6* **44,** 1152-1159.

28. Ridgway,C.J. and Gane,P.A.C.: 2002, Dynamic absorption into simulated porous structures, *Colloids and Surfaces A: Physicochemical and Engineering Aspects* **206,** 217-239.

29. Ridgway,C.J., Gane,P.A.C., and Schoelkopf,J.: 2002, Effect of capillary element aspect ratio on the dynamic imbibition with porous networks, *Journal of Colloid and Interface Science* **252,** 373-382.

30. Ridgway,C.J., Ridgway,K., and Matthews,G.P.: 1997, Modelling of the Void Space of Tablets Compacted over a Range of Pressures, *Journal of Pharmacy and Pharmacology* **49,** 377-383.

31. Ridgway,C.J., Schoelkopf,J., Matthews,G.P., Gane,P.A.C., and James,P.W.: 2001, The effects of void geometry and contact angle on the absorption of liquids into porous calcium carbonate structures, *Journal of Colloid and Interface Science* **239,** 417-431.

32. Schoelkopf,J., Gane,P.A.C., Ridgway,C.J., and Matthews,G.P.: 2000b, Influence of Inertia on Liquid Absorption into Paper Coating Structures, *Nordic Pulp and Paper Research Journal* **15,** 422-430.

33. Schoelkopf,J., Gane,P.A.C., Ridgway,C.J., and Matthews,G.P.: 2002, Practical observation of deviation from Lucas-Washburn scaling in porous media, *Colloids and Surfaces A: Physicochemical and Engineering Aspects* **206,** 445-454.

34. Schoelkopf,J., Ridgway,C.J., Gane,P.A.C., Matthews,G.P., and Spielmann,D.C.: 2000a, Measurement and network modelling of liquid permeation into compacted mineral blocks, *Journal of Colloid and Interface Science* **227,** 119-131.

35. Sorbie,K.S., Wu,Y.Z., and McDougall,S.R.: 1995, The extended washburn equation and its application to the oil/water pore doublet problem, *Journal of Colloid and Interface Science* 289-301.

36. Szekely,J., Neumann,A.W., and Chuang,Y.K.: 1971, The rate of capillary penetraion and the applicability of the Washburn equation, *Journal of Colloid and Interface Science* **35,** 273-278.

37. Taylor,S.C., Hall,Ch., Hoff,W.D., and Wilson,M.A.: 2000, Partial Wetting in Capillary Liquid Absorption by Limestones, *Journal of Colloid and Interface Science* 351-357.

38. van Oss,C.J., Giese,R.F., Li,Z., Murphy,K., Norris,J., Chaudhury,M.K., and Good,R.J.: 1992, Determination of contact angles and pore sizes of porous media by column and thin layer wicking, *Journal of Adhesion Science and Technology* 413-428.

39. Washburn,E.W.: 1921, The dynamics of fluid flow, *Physical Review* **17,** 273-283.

40. Yang,Y.-W., Zografi,G., and Miller,E.E.: 1988, Capillary flow phenomena and wettability in porous media, *Journal of Colloid and Interface Science* **122,** 35-46.